Research Article | Vol. 13, No. 1 / 1 Jan 2023 / Optical Materials Express 41
Optical Materials EXPRESS

Opto-thermal dynamics of thin-film optical limiters based on the VO_2 phase transition

Andrea Tognazzi,[1,2,*] Marco Gandolfi,[2,3,4] Bohan Li,[5] Gina Ambrosio,[2] Paolo Franceschini,[2] Rocio Camacho-Morales,[5] Alfonso Carmelo Cino,[1] Camilla Baratto,[2] Domenico de Ceglia,[2,3,4] Dragomir Neshev,[5] and Costantino De Angelis[2,3,4]

[1]*Department of Engineering - University of Palermo, Viale delle Scienze ed. 9, Palermo, 90128, Italy*
[2]*Istituto Nazionale di Ottica - Consiglio Nazionale delle Ricerche, Via Branze 45, Brescia, 25123, Italy*
[3]*Department of Information Engineering - University of Brescia, Via Branze 38, Brescia, 25123, Italy*
[4]*Consorzio Nazionale Interuniversitario per le Telecomunicazioni (CNIT), Viale G.P. Usberti 181/A Sede Scientifica di Ingegneria-Palazzina 3, 43124 Parma, Italy*
[5]*ARC Centre of Excellence for Transformative Meta-Optical Systems (TMOS), Research School of Physics, The Australian National University, Canberra ACT 2601, Australia*
[*]*andrea.tognazzi@unipa.it*

Abstract: Protection of human eyes or sensitive detectors from high-intensity laser radiation is an important challenge in modern light technologies. Metasurfaces have proved to be valuable tools for such light control, but the actual possibility of merging multiple materials in the nanofabrication process hinders their application. Here we propose and numerically investigate the opto-thermal properties of plane multilayered structures with phase-change materials for optical limiters. Our structure relies on thin-film VO_2 phase change material on top of a gold film and a sapphire substrate. We show how such a multi-layer structure can act as a self-activating device that exploits light-to-heat conversion to induce a phase change in the VO_2 layer. We implement a numerical model to describe the temporal evolution of the temperature and transmittivity across the device under both a continuous wave and pulsed illumination. Our results open new opportunities for multi-layer self-activating optical limiters and may be extended to devices based on other phase change materials or different spectral regions..

1. Introduction

The quest to achieve dynamic control of nanoscale optical devices is at the forefront of scientific investigation in photonics. In the past years, a plethora of solutions, including liquid crystals, hot electrons, materials with large nonlinear and electro-optical coefficients, mechanical strain, and phase change materials (PCM), have been proposed to tune the radiation properties or enhance the field confinement in nanostructured devices such as nanoantennas and metasurfaces [1–4]. In particular, PCMs have shown great versatility since they can be integrated within nanoscale devices and allow for dynamic control with different stimuli along with large contrast of the optical constants between the two phases [5–10]. Within the family of PCMs today available, vanadium dioxide (VO_2) stands out due to its abrupt dielectric to metal transition at $\sim 70°C$, which can be induced thermally, electrically or optically [11–13]. In this way, depending on the external control source, it is possible to switch the phase of the device on different timescales ranging from picoseconds to seconds [14–16]. An important application of PCM is the optical limiter used to prevent damage in detection devices or protect eyes from coherent radiation [17,18]. In this framework, a fast, self-activating device is needed to achieve a reliable protection tool. Nanoantennas and metasurfaces have been extensively investigated to perform beam steering, polarization control, sensing and nonlinear frequency mixing, thus showing the

#472347 https://doi.org/10.1364/OME.472347
Journal © 2023 Received 2 Aug 2022; revised 20 Oct 2022; accepted 31 Oct 2022; published 6 Dec 2022

Optical Materials EXPRESS

possibility to implement unique and non-trivial functionalities which are not available in thin films [19–21]. Recent works incorporated VO_2 to dynamically tune, by means of an external trigger, the transmission of metasurfaces [22,23] and perform dynamic polarization control [24,25]. VO_2-based nanostructured devices have also been employed to perform optical limiting in the infrared region. Broadband optical limiting above 2 μm was reported in [26], while in [18] the authors achieved 25.2 dB turn down ratio around 1200 nm with shorter bandwidth (~20 nm). However, the complexity in the fabrication process itself and the need to maintain a high resolution (on the order of tens of nanometers) on large samples may hinder the large scale production via standard fabrication techniques, such as deep UV photolitography [19–21]. Furthermore, mixing materials to achieve dynamic control makes the fabrication process, such as electron beam litography, even more difficult and delicate [18,22,23,27]. In stark contrast to nanostructured metasurfaces, thin-film planar multilayers, which are composed by stacking a few nano-scale films of different materials on top of each other, have lower versatility but feature large area, easier and faster fabrication processes compatible with industrial needs. Indeed, such multi-layer structures have already been employed to build smart windows, perfect mirrors, compact modulators and filters [28,29].

Here, a multilayered structure composed of a VO_2 film stacked on a thin gold (Au) layer on a sapphire (Al_2O_3) substrate is proposed and its thermo-optical properties are studied. The gold film provides an efficient way to increase the radiation absorption inside the VO_2 and induces thermal switching upon controlled illumination intensity on shorter timescales. First, by employing a Transfer matrix approach we maximize the transmittivity contrast of the device when the VO_2 changes from dielectric to metallic phase. Then, we implement a numerical model that takes into account the mutual influence between light and heat propagation on the VO_2 optical properties, extending previous models which considered VO_2 phase transition as a step function of the temperature and did not consider latent heat during the phase transition [14,30]. Next, we numerically investigate the transient response of the device upon illumination with a train of laser pulses (wavelength λ = 1550 nm), and the influence of the light intensity, pulse duration and repetition rate on the device response. Finally, the characteristic time and number of pulses needed to achieve steady optical transmission reduction under pulsed illumination were determined. To the best of our knowledge, our work provide the first study of multiple pulses temporal dynamics of temperature and transmittivity in a self activating PCM based device. The results provide an easy-to-grow and robust multilayer device for a self-activating optical limiter. The adopted limiting scheme may be easily extended to other PCMs, other spectral regions and nanostructured devices such as nanoantennas and metasurfaces.

2. Design

In order to design an efficient self-activating optical limiter, it is crucial to control the threshold intensity at which the phase transition in VO_2 occurs. The design depicted in Fig. 1(a) may prove useful for this purpose, thanks to the presence of the thin gold layer. The latter acts as a reflector to enhance the electromagnetic field inside the PCM. In contrast to Ref. [31], here we place the gold layer between the VO_2 and the substrate because this configuration allows to maximize the transmittivity contrast when impinging from the VO_2 side.

The optimization of the geometrical parameters is performed by employing a Transfer matrix (T-matrix) approach. In a nutshell, a plane wave impinges on the device from the air side (top of the device), as shown in Fig. 1(a). The device is illuminated at normal incidence. The light transmittivity (Tr) is calculated in two cases: (*i*) when the VO_2 layer is fully in the dielectric phase ("on" state) or (*ii*) when the entire VO_2 layer is in the metallic phase ("off" state). For these calculations we adopt the refractive index of the VO_2 in the dielectric and metallic phases, reported in [30]. The refractive indices of the gold and the sapphire are taken from Ref. [32] and

Optical Materials EXPRESS

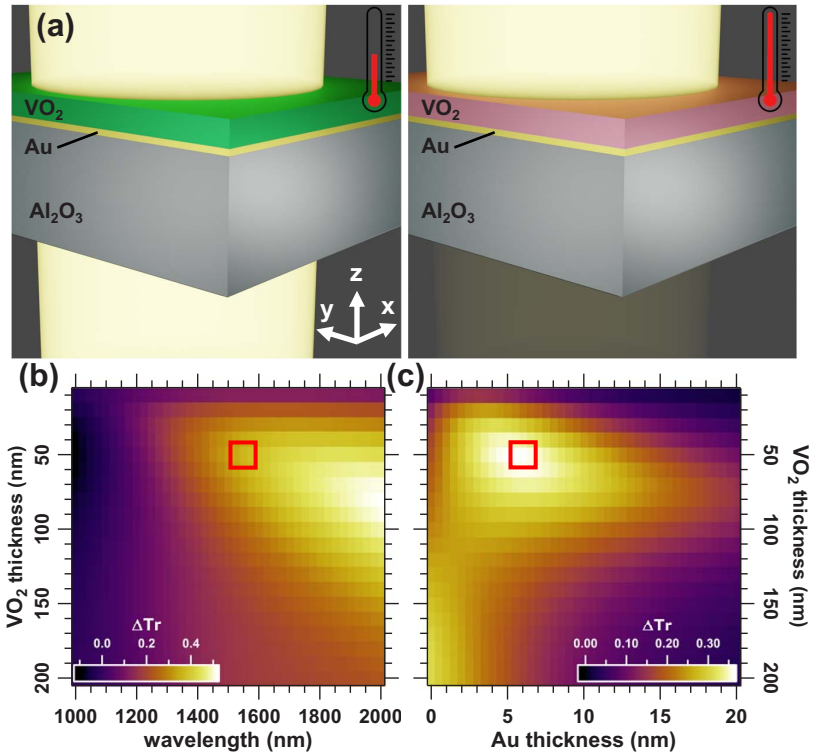

Fig. 1. (a) Pictorial sketch of the device. Left is when the VO_2 layer is fully in the dielectric phase ("on" state) and right is when the entire VO_2 layer is in the metallic phase ("off" state). (b) Transmittivity difference ΔTr (colour scale) as a function of the wavelength (λ) and VO_2 film thickness, for a fixed Au thickness of 5 nm. (c) Transmittivity difference (colour scale) as a function of Au and VO_2 film thickness, for a fixed wavelength λ = 1550 nm. The transmittivity difference is defined as $\Delta Tr = Tr_{diel} - Tr_{met}$. The red squares correspond to the optimal configuration at λ = 1550 nm.

Ref. [33], respectively. See supplementary material for more details about possible fabrication techniques and optical characterization.

The transmittivity difference $\Delta Tr = Tr_{diel} - Tr_{met}$ between the dielectric and metallic phases as a function of the incident light wavelengths is reported in Fig. 1(b). In this case a fixed thickness of 5 nm is considered for the gold thin film layer. We observe that ΔTr increases at longer wavelength since the difference between the imaginary parts of the VO_2 refractive index in the two phases becomes larger. Since the dielectric phase has non-zero imaginary part, increasing the VO_2 thickness beyond $\sim \lambda/20$ decreases the transmittivity in the "on" state and thus ΔTr also decreases. Furthermore, a thicker gold film provides a larger heating source, which may help to reduce the intensity threshold and the transmittivity value in the "on" state; however, this occurs at the cost of a reduced transmittivity contrast and transmittivity in the "off" state. We choose a working wavelength of 1550 nm since it is a standard in optical communications. Nevertheless, our device can achieve comparable performances at longer wavelengths, resulting in larger bandwidth applications. In Fig. 1(c), we report the gold and VO_2 thickness optimization at 1550 nm, which gives an optimal thickness of 6 nm and 52 nm, respectively. The device has comparable performances also at non-normal incidence since it is not based on the shift of sharp resonances (see Fig. S2 and S3).

Optical Materials EXPRESS

3. Opto-thermal simulations

Once we have obtained the optimal configuration for optical limiting, we study the *self-activating performance* of the device under a dynamic excitation (i.e. transient illumination). We introduce a fully-coupled opto-thermal model to quantify the thermal dynamics in the system and its repercussion on the optical properties of the structure during the phase transition of the VO_2 layer. The full opto-thermal problem is solved using the finite-element method (FEM) in COMSOL Multiphysics [34,35].

Due to the transverse symmetry of the structure, we consider a 2D geometry (a cross-sectional plane $x-z$ in Fig. 1(a)) to reduce the computation time. The geometry includes four domains: a top air domain (with refractive index $n = 1$), a VO_2 and a gold layer, and a sapphire substrate.

We start solving the problem from the optical part and then we calculate the heat generated due to light-to-heat conversion to compute the variation of the optical properties of VO_2. This process is iteratively repeated up to convergence. While solving the optical problem we monitor the device transmittivity and compute ohmic losses. We illuminate the structure with a plane wave in air at normal incidence of wavelength 1550 nm and intensity I_0.

The problem shows a translation symmetry along the x-direction, hence, we introduce periodic boundary conditions (Floquet periodicity) on the vertical sides [36]. The horizontal width of the geometry is set to 800 nm. The optical problem is solved with a frequency-domain study and the solution allows to compute the absorbed power density (averaged over one temporal cycle) as $Q_h(\mathbf{r}) = Re[\tilde{\mathbf{J}}(\mathbf{r}) \cdot \tilde{\mathbf{E}}^*(\mathbf{r})]/2$, where $\tilde{\mathbf{E}}^*$ and $\tilde{\mathbf{J}}$ are the complex-conjugate of the electric field and the complex valued current density, respectively, *Re* denoting the real part of the complex value [37].

The absorbed power density allows to quantify the heat source term to be assigned to VO_2 and gold domains in the thermal problem. Note that the light absorption in the substrate is neglected, hence its refractive index is entirely real. To model the thermal problem, we solve the diffusion equation [37] in the VO_2, gold and substrate domains. On the lateral sides we assign adiabatic boundary conditions. Indeed, the problem is symmetrical in the xy-plane and hence the only non-zero component of the heat flux is along z. To limit the computational burden, the thermal problem was not solved in the air domain. The presence of the air was accounted for by assigning on the interface air-VO_2 a radiation boundary condition $\mathbf{q} \cdot \mathbf{n} = \sigma\epsilon \left(T^4 - T_{amb}^4\right)$ and a convection boundary condition $\mathbf{q} \cdot \mathbf{n} = h\,(T - T_{amb})$, where $\mathbf{q}$ is the heat flux, $\mathbf{n}$ is the unit normal vector pointing outside the domain, $\sigma = 5.67 \times 10^{-8}$ W/m^{2}K^4 is the Stefan-Boltzmann constant, $\epsilon \approx 1$ is the emissivity, $h \approx 25$ W/m^{2}K is the convective heat transfer coefficient (free convection in air is assumed [38]) and $T_{amb} = 293.15$ K is the external ambient temperature. The same radiation and convection boundary conditions have been assigned on the bottom face of the substrate as well, since it is assumed to be in contact with air.

The simulation parameters are reported in Table 1. The specific heat per unit mass of the VO_2 is reported for temperatures far from the phase transition. Indeed, VO_2 is endowed with a first order phase transition with the presence of latent heat across the phase transition. As a consequence, around the critical temperature, the specific heat is a function of the temperature [39]. The developed model accounts for the presence of the latent heat, which is usually neglected even if it plays a significant role on shorter relaxation timescales.

Table 1. Mass density ρ, thermal conductivity κ_T and specific heat per unit mass C_p for VO_2, Au and Al_2O_3. The VO_2 and Au thermal parameters are taken from Ref. [28] and [42], respectively. In this table we reported the specific heat of the VO_2 far from the phase transition.

Parameters	VO_2	Au	Al_2O_3
ρ [kg/m^3]	4600	19300	3900 ([40])
κ_T [W m^{-1} K^{-1}]	6	317	40 ([41])
C_p [J kg^{-1} K^{-1}]	690	129	775 ([41])

Optical Materials EXPRESS

In the model we neglected the variations of thermal conductivity (κ_T) and mass density (ρ) of the VO_2 across the phase transition. We also neglected the thermal conductivity reduction in thin films due to ballistic effect and the thermal boundary resistance at the interface among the involved materials (in analogy with Ref. [43]). Indeed, the presence of these refinements would complicate tremendously the model without affecting the results significantly.

As we will see later, the thermal problem may be solved with a stationary or time-dependent solver. The obtained temperature is used to modify the dielectric function of the VO_2 layer. In the latter domain, the effective complex dielectric function ε_{eff} depends on the fractions of the VO_2 in the dielectric and metallic phases, which in turns depend on the temperature according to the Looyenga mixing rule [30]:

$$[\varepsilon_{\text{eff}}(\lambda, T)]^s = [1 - f(T)]\,[\varepsilon_{\text{diel}}(\lambda)]^s + f(T)\,[\varepsilon_{\text{met}}(\lambda)]^s\,, \tag{1}$$

where $\varepsilon_{\text{diel}}$ and ε_{met} are the complex dielectric functions of VO_2 in the dielectric and metallic phase, respectively, $s = 1/3$ and the fraction of the metallic phase is given by:

$$f(T) = \left\{1 + \exp\left[\frac{W}{k_B}\left(\frac{1}{T} - \frac{1}{T_c}\right)\right]\right\}^{-1}, \tag{2}$$

with $W = 4.85$ eV and $T_c = 75.1$°C. We point out that the effective dielectric constant in VO_2 might be described properly also with a Bruggeman effective medium theory [44], rather than with the Looyenga mixing rule [30]. However, the analytical expression for ε_{eff} in the Bruggeman formalism is more complicated and might hinder the convergence of the solution. For this reason, we used the much simpler expression obtained with the Looyenga mixing rule.

Equation (1) allows to describe the spatial profile of the VO_2 refractive index modified by the thermal dynamics. With this information, the electromagnetic problem is computed again. The FEM model solves the electromagnetic and thermal physics at the same time, finding a self-consistent solution for this nonlinear problem.

The thickness of the air domain for the optics is taken as 2 μm and truncated with a port boundary condition, which introduces the light beam in the system. The substrate thickness for the thermal problem is taken as ≈ 7 μm so as to mimic real samples. To limit the computational burden, the optical problem was solved on a much shorter substrate (≈ 3 μm), that was truncated with a port boundary condition with no light entering in the computation cell from it.

We used a triangular mesh, whose maximum element size is shorter than $1/7$ of the light wavelength in each domain. To guarantee the accuracy of the obtained solution, in the short VO_2 and Au domains the maximum element size was reduced to $1/5$ of the domain thickness.

Steady-state simulation. Before modelling a complete temporal evolution inside the device, we consider the simpler case of illumination with continuous light. In this case, the thermal problem needs a stationary solver to find the equilibrium solution. The heat source is the absorbed power density $Q_h(\mathbf{r})$ computed from the optical problem. The opto-thermal problem is solved with a frequency-stationary solver.

Time-dependent simulation. In this case we model the transient response of the device upon a time-varying light illumination. The system starts from an equilibrium condition, where the temperature is set at room temperature $T_{\text{amb}} = 293.15$ K everywhere and hence the device is in the "on" state. In this equilibrium situation, we assume that the source term in the thermal problem is zero. Afterwards, to model the thermal dynamics in the device, we assign a time-dependent source term in the VO_2 and gold domains of the type $G(t)Q_h(\mathbf{r})$, where $G(t)$ is a function accounting for the temporal evolution and $Q_h(\mathbf{r})$ is the absorbed power density computed with the optical problem. This source terms triggers the thermal dynamics, in turns altering the refractive index of the VO_2 domain and yielding the transient limiting performance.

We consider two possible scenarios for the transient excitation: the first is the switch on of a continuous wave excitation. This case aims at studying the response of the device initially in the

Optical Materials EXPRESS

"on" state and at a time t_0 a hazardous continuous light is turned on. Hence, we set $G(t) = H(t-t_0)$, where H is the Heaviside step function. We compute the temporal dynamics, bringing the device from the initial rest state to the final steady-state-like condition. In practice, this case represents the transient evolution of the device just after the switch on of a CW light until the steady state condition is reached. The second scenario corresponds to the illumination with a train of multiple pulses. In this regime, the device is initially in the "on" state and, afterwards, it is excited by a train of pulses (with repetition rate RR). We note that any pulse shape may be introduced in the model at the expense of computation time to reach convergence. Although mode-locked laser pulse shape is described by a $sech^2$ function, we employed a Gaussian line shape since it is very similar but gives better convergence results. Hence, we choose a time-dependent light intensity profile of the form:

$$G(t) = \sum_{m=1}^{N} \exp\left\{-4\ln(2)\left[\frac{t - t_0 - (m-1)/RR}{\tau}\right]^2\right\}, \tag{3}$$

where τ is the temporal full-width at half maximum (FWHM) of the pulse, t_0 is the pulse central time [42] and N is the number of pulses (the case with $N = 1$ corresponds to a single pulse illumination). We usually set $t_0 = 10\tau$ to avoid conflicts with the initial conditions of equilibrium at room temperature. In practice, this scenario mimics the device response in the case of illumination with a pulsed laser source.

The control parameter of the energy entering from the port is the light energy density Φ (averaged over time). Hence, the light intensity set on the port is $I_0 = \Phi\sqrt{4\ln(2)/(\pi\tau^2)}$. We compute the temporal dynamics to study the device excitation due to each pulse and the subsequent relaxation.

The problem is solved with a frequency-transient solver. To help the convergence, a frequency study step is solved prior to tackle the frequency-transient study step. In order to have a precise solution in a reasonable computation time, the time step is adapted to be very short around the transient changes of the excitation and coarser during the slower cooling process. In particular, in the switch on case we approximate the Heaviside step function with a function smoothly increasing from 0 to 1 around the switch on time t_0. The extension of the temporal duration where the smooth transition occurs is taken as 2 ps, a very short interval with respect to the cooling time. The time step along the smooth transition is smaller than the duration of the transition itself. Instead, for the pulsed excitation, during the time instants of the pulse duration the time step is set as 1/10 of the pulse temporal FWHM. In both cases, the time step is progressively released during the cooling process to have 100 temporal points in every temporal decade.

4. Results

Latent heat, which is often neglected in the literature, is the energy released or absorbed by a body during a first order phase transition. In our work, we study first the influence of latent heat on the maximum temperature reached in the VO_2 layer and we show its influence upon the cooling dynamics. Secondly, we study the device behavior for different pulse energies, at fixed pulse duration, in order to obtain the threshold intensity for self-activated switching of the device. Then we show that there is an optimum pulse duration maximizing the temperature increase in the VO_2. Lastly, we show the activation dynamics when a train of pulses, which is usually generated in mode-locked and Q-switched lasers, impinges on the device.

4.1. Single pulse

In Fig. 2(a) we report the temperature (left axis, red curves) in the middle of the VO_2 layer and the transmittivity (right axis, blue curves) as functions of time. A temporal Gaussian pulse with energy density $\Phi = 10$ mJ/cm^2 and temporal width of $\tau = 20$ ps impinges on the device. The

Optical Materials EXPRESS

solid (dashed) red and blue lines are obtained including (neglecting) the latent heat λ_h. The shaded grey region indicates temperatures below the critical temperature $T_c \sim 75°C$ [30]. From Fig. 2(a), it is clear that the inclusion of the latent heat lowers the maximum temperature achieved inside the VO_2 and thereby the threshold intensity required to switch the device increases. Indeed, part of the pulse energy is employed to modify microscopically the VO_2 layer to bring it to the new phase, thus lowering the maximum temperature. Figure 2(a) also suggests that the time necessary to recover the initial rest condition is different for transmittivity and temperature. Indeed, the transmittivity is determined by the phase of VO_2 rather than the exact temperature value, thus the critical time is the time after which the temperature decreases below the critical value, rather than the time necessary to retrieve the room temperature in all the device.

The energy stored in the latent heat is released during the cooling process, thus slowing down a bit the latter (see the shoulder appearing in the red curve in the time span between 1 ns and 10 ns). When the latent heat is included in the simulations, we observe that the device stays in the "off" state for a longer time. We will exploit this behavior for the analysis of multiple pulses excitation. Since the presence of the latent heat is more realistic and useful for optical limiting purposes, from now on, we always include it in the modelling.

In Fig. 2(b) we report the temporal evolution of the temperature in the middle of the VO_2 layer for different peak intensities of a 20 ps laser pulse. For I_0<150 MW/cm^2, the critical temperature is not reached and thus the device does not activate. For $I_0 \sim 150$ MW/cm^2, there is a plateau temperature dictated by the presence of the latent heat and the heat propagation time. For I_0>150 MW/cm^2, the maximum temperature is not reached immediately after the pulse arrival, but ~ 300 picoseconds later. To further understand this behaviour, in Fig. 2(c) we report the temperature as a function of time and position within the multilayer (z-axis). The horizontal dashed line denotes the middle of VO_2 layer. It is clear that the major amount of heat is generated after a few picoseconds in proximity of the air-VO_2 interface (top left of the figure), which presents the higher temperature values (see also Fig. S1). For longer times, heat propagates toward the substrate and the temperature profile along the vertical axis becomes homogeneous, as expected for thermal equilibrium. We highlight the role of the gold layer, since shortly after the pulse arrives, in its proximity, the temperature increases due to the fact that this layer acts not only as a mirror that enhances the electromagnetic field in the VO_2 film, but also as a heat source (see Fig. 2(c)-(d)). The maximum temperature inside the substrate is achieved at longer time delays, which depends on the z-coordinate. This further confirms that the main dissipation channel of heat is the substrate, whose thermal properties play a key role in determining relaxation time.

In Fig. 3 we report the temperature as a function of time for different pulse duration at the same energy density. The shaded colored areas are the Gaussian pulses impinging at time $t_0 = 10\tau$. We note that in the time span δt, the heat covers a distance $d \sim \sqrt{\alpha \delta t}$, where $\alpha = \kappa_T/(\rho C_p)$ is the thermal diffusivity. Hence, the time necessary for the heat to escape from the center of the VO_2 layer to the gold and substrate scales as $(d_{VO_2}/2)^2/\alpha_{VO_2} \sim 230$ ps. For these reasons, in the case of the curves reported in Fig. 3 for $\tau \geq 500$ ps, the heat escapes from the VO_2 layer while the pulse is still illuminating the sample. This heat diffusion explains the fact that the maximum temperature is lower for longer pulses, since part of the pulse energy is dissipated towards the substrate already during light illumination.

For τ smaller than 200 ps all the maximum T are achieved after ~ 300 ps following the time instant t_0, the latter being the time that heat takes to propagate from the top part of VO_2 (where the spatial maximum of the temperature is recorded) toward the center of the film. Indeed, since the major part of the pulse is absorbed at the interface VO_2-air, once the pulse ends, the temperature in the middle is still increasing due to heat diffusion from the VO_2-air interface toward the gold film. If $\tau \sim 10$ ps, the energy coming from the top interface of the device due to heat diffusion, and the energy delivered by the pulse sum up at the same instant and the temperature increase is

Optical Materials EXPRESS

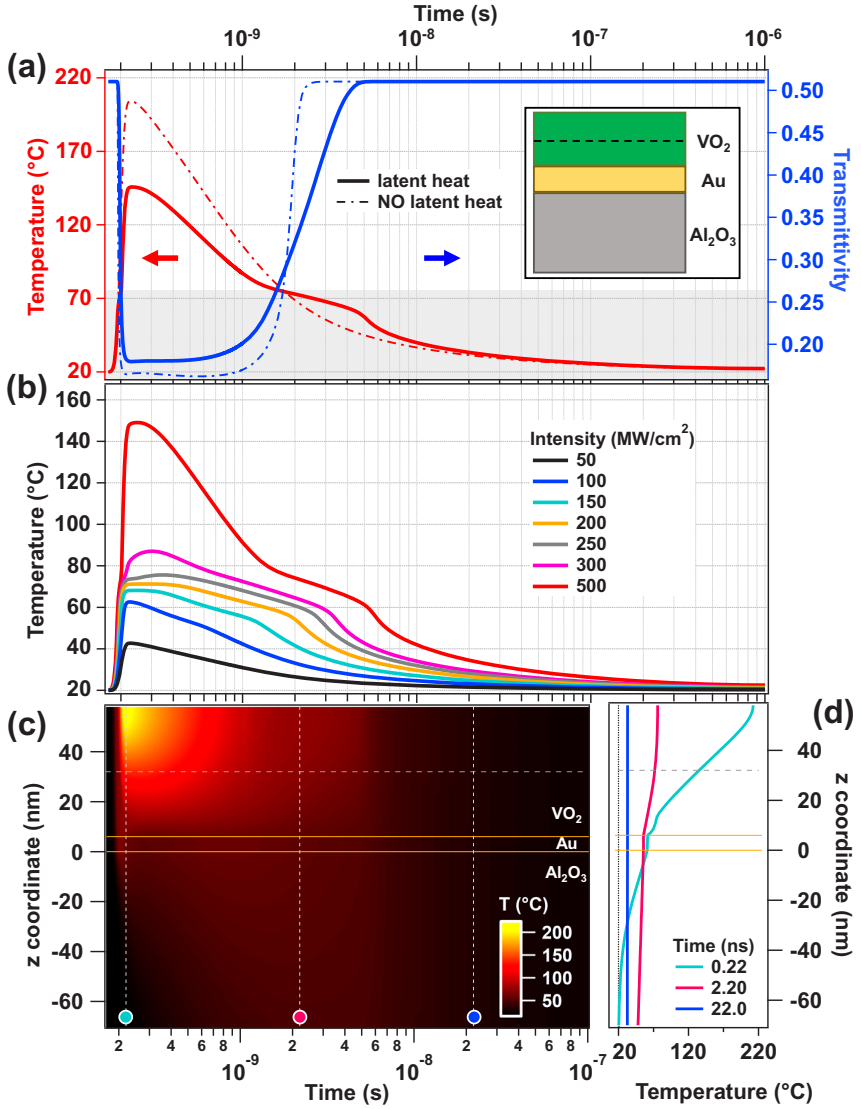

Fig. 2. (a) Temperature (red left axis) and transmittivity (blue right axis) as a function of time with single pulse illumination (τ = 20 ps, Φ = 10 mJ/cm^2). The continuous line takes into account the latent heat of the first order phase transition of VO_2. The shaded area corresponds to temperatures lower than the critical temperature. (b) Temperature as a function of time for different pulse intensities at fixed pulse duration τ = 20 ps. (c) Temperature (T) as a function of position (vertical axis) and time (horizontal axis). The vertical dashed white lines with color circular markers denote the time values at which the temperature profiles displayed in panel d are taken. The yellow horizontal line corresponds to the VO_2/Au and Au/sapphire interfaces. (d) Temperature profile inside the multilayer at different time instants: 0.22 (light blue solid line), 2.2 (magenta solid line), and 22.0 ns (dark blue solid line). In panels c and d, the horizontal dashed line denotes the middle of VO_2 layer and the solid yellow lines define the Au layer.

Optical Materials EXPRESS

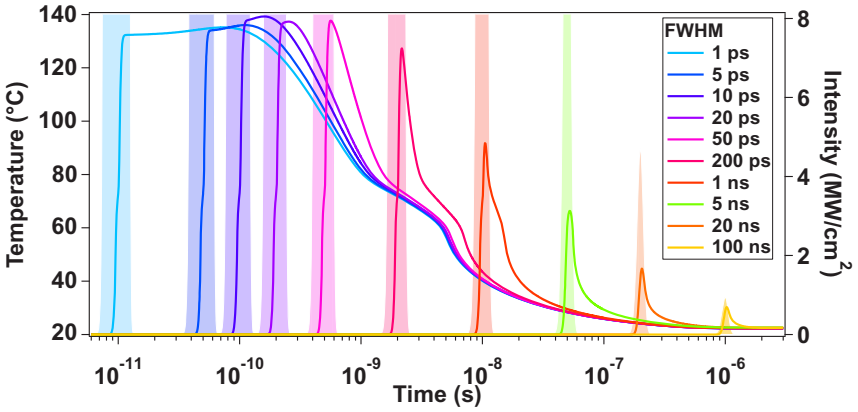

Fig. 3. Temperature as a function of time (in log scale) for different pulse duration. The colored shades represent the Gaussian pulse impinging on the device at time $t_0 = 10\tau$ and energy density Φ =100 J/m^2.

maximized. At longer time delays, below the critical temperature, the cooling dynamics does not depend upon the pulse duration and follows an exponential decay as expected for heat diffusion.

4.2. *Train of pulses*

Many practical applications, however, do not rely on single pulses, but rather on a train of pulses with constant repetition rate. Therefore, we turn our attention to the response of the device when a train of finite number of pulses impinges on it. To do this, we consider a train of temporal pulses with FWHM τ = 20 ps and energy density Φ = 20 mJ/cm^2. We vary the time delay between the pulses (correspondingly the repetition rate). In Fig. 4(a) we report the temperature in the middle of the VO_2 layer (solid red line, left axis) and the device transmittivity (solid blue line, right axis) as function of time for 20 laser pulses with a time-delay of 0.1 µs. For the first pulse, the temperature temporal dynamics is the same as in the case of a single pulse. However, before the complete cooling occurs (i.e. when the temperature is still higher than T_{amb}), the second pulse hits the structure. In this way, the maximum temperature reached after the second pulse is higher than the maximum temperature after the first one. After multiple pulses, the heat accumulation prevents the temperature to decrease below T_c in the time between individual pulses. Hence, as long as the train of pulses is active, the device stays permanently in the "off" state, thus limiting the transmitted light of the subsequent pulses.

As a comparison, Fig. 4(a) shows (dashed lines) the temperature and transmittivity dynamics in the case of continuous wave (CW) illumination with intensity $I_0 = \Phi \cdot RR$. It is clear that the minimum temperature reached after the cooling in the pulse regime resembles the same trend of CW illumination. However the "off" state is reached in shorter time in the CW configuration. This is due to the fact that we are considering the same energy density impinging on the structure, thus the electromagnetic field continuously transfers energy to the device, unlike in the pulsed regime. It is clear that lower repetition rates require more pulses to induce a permanent "off" state since part of the heat generated by light absorption is dissipated in the substrate before the next pulse impinges on the device.

In Fig. 4(b), we report the number of pulses needed to achieve the permanent "off" state as a function of the repetition rate. We note that for low repetition rates the number of pulses needed to induce the switch weakly depends on the repetition rate. This is due to the fact that the device cooling follows a decreasing exponential decay below the critical temperature and thus at long time delays the temperature dependence on time is mild. On the other hand, at high repetition

Optical Materials EXPRESS

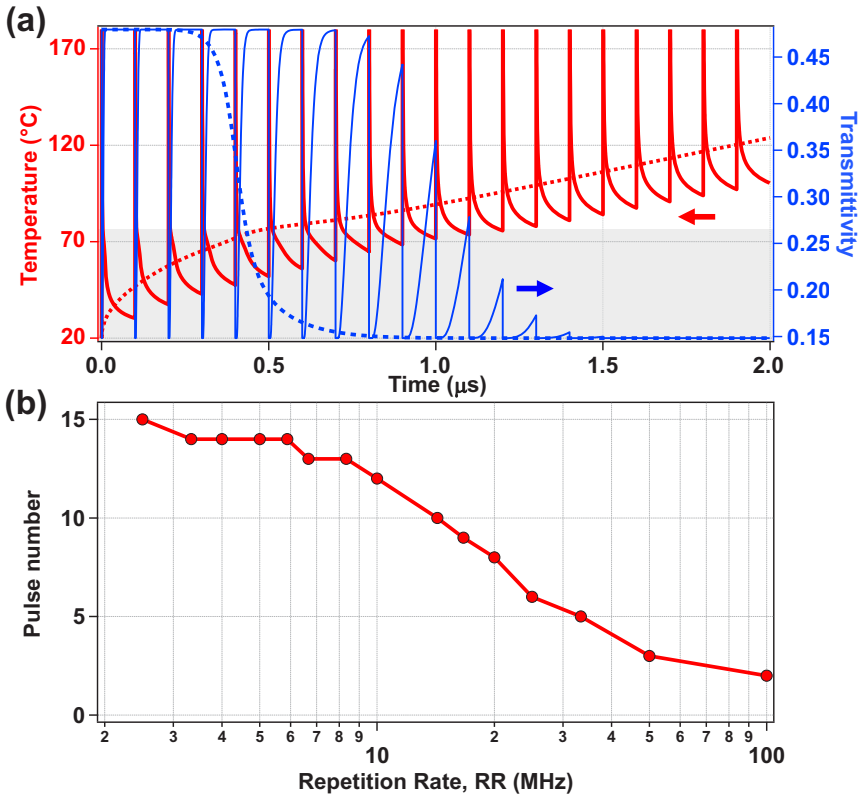

Fig. 4. (a) Temperature (red, left axis) and transmittivity (blue, right axis) temporal evolution. Solid lines denote the temporal dynamics for pulsed illumination with τ=20 ps, repetition rate RR=10 MHz, and Φ=20 mJ/cm^2. Dashed lines denote the temporal dynamics for continuous illumination with Φ=20 mJ/cm^2 and $I_0 = \Phi \cdot RR$=0.2 MW/cm^2. The shaded area corresponds to temperatures lower than the critical temperature. (b) Number of pulses necessary to achieve the "off" state as the initial condition at different repetition rates.

rates the number of pulses needed to induce the phase switch strongly depends on the repetition rate since during the initial cooling the temperature decrease is very fast.

5. Conclusions

In this article we proposed a VO_2-gold-sapphire multilayer structure for optical limiting. We optimized the structure with a Transfer Matrix approach to maximize the transmittivity contrast of the limiter upon VO_2 phase transition. We developed a numerical model to study the transient limiting performances of the device. We include the latent heat related to the phase transition in VO_2, enriching the description provided by previous models employed in the literature, and the refractive index temperature dependence due to light absorption. We considered both pulsed and continuous wave illumination. We showed that the maximum temperature increase in the middle of VO_2 layer does not occur exactly when the pulse intensity is maximum but depends also on the heat propagation into the device. We highlight that including the latent heat results in higher threshold intensities to activate the device and longer relaxation dynamics. We provided the first numerical study, to the best of our knowledge, of multiple pulse illumination of a phase

Optical Materials EXPRESS

change material based device and we showed that it is possible to perform optical limiting upon illumination with multiple pulses.

Our results pave the way to a different approach in the design of optical limiting and dynamically self-reconfigurable devices dedicated to pulsed laser sources. Indeed, the modelling approach presented here is a key element to design a limiter with the desired properties. The approach is easily applicable to different phase-change materials, different operating wavelengths and substrate materials.

Funding. Australian Research Council (CE200100010); North Atlantic Treaty Organization (SPS G5850).

Acknowledgments. The authors acknowledge the financial support by NATO SPS, the Australian Research Council Centres of Excellence Program (CE200100010). We thank A. Sukhorukov for the useful discussions. A. T. acknowledges the financial support by European Union "FESR o FSE, PON Ricerca e Innovazione 2014-2020 - DM 1062/2021".

Disclosures. The authors declare no conflicts of interest.

Data availability. Data are available upon request to the authors.

Supplemental document. See Supplement 1 for supporting content.

References

1. D. Rocco, L. Carletti, R. Caputo, M. Finazzi, M. Celebrano, and C. D. Angelis, "Switching the second harmonic generation by a dielectric metasurface via tunable liquid crystal," Opt. Express **28**(8), 12037–12046 (2020).
2. T. Lewi, P. P. Iyer, N. A. Butakov, A. A. Mikhailovsky, and J. A. Schuller, "Widely tunable infrared antennas using free carrier refraction," Nano Lett. **15**(12), 8188–8193 (2015).
3. L. Carletti, M. Gandolfi, D. Rocco, A. Tognazzi, D. de Ceglia, M. A. Vincenti, and C. D. Angelis, "Reconfigurable nonlinear response of dielectric and semiconductor metasurfaces," Nanophotonics **10**(17), 4209–4221 (2021).
4. S. V. Makarov, A. S. Zalogina, M. Tajik, D. A. Zuev, M. V. Rybin, A. A. Kuchmizhak, S. Juodkazis, and Y. Kivshar, "Light-induced tuning and reconfiguration of nanophotonic structures," Laser Photonics Rev. **11**(5), 1700108 (2017).
5. J. del Valle, J. G. Ramírez, M. J. Rozenberg, and I. K. Schuller, "Challenges in materials and devices for resistive-switching-based neuromorphic computing," J. Appl. Phys. **124**(21), 211101 (2018).
6. Y. Zhang, C. Fowler, J. Liang, B. Azhar, M. Y. Shalaginov, S. Deckoff-Jones, S. An, J. B. Chou, C. M. Roberts, V. Liberman, M. Kang, C. Ríos, K. A. Richardson, C. Rivero-Baleine, T. Gu, H. Zhang, and J. Hu, "Electrically reconfigurable non-volatile metasurface using low-loss optical phase-change material," Nat. Nanotechnol. **16**(6), 661–666 (2021).
7. A. Mandal, Y. Cui, L. McRae, and B. Gholipour, "Reconfigurable chalcogenide phase change metamaterials: a material, device, and fabrication perspective," JPhys Photonics **3**(2), 022005 (2021).
8. D.-Q. Zhang, G.-M. Pan, Z.-W. Jin, F.-Z. Shu, X.-F. Jing, Z. Hong, and C.-Y. Shen, "Tunable dielectric metasurfaces by structuring the phase-change material," Opt. Express **30**(3), 4312–4326 (2022).
9. A. Tognazzi, A. Locatelli, M. A. Vincenti, C. Giannetti, and C. De Angelis, "Tunable optical antennas using vanadium dioxide metal-insulator phase transitions," Plasmonics **14**(5), 1283 (2019).
10. Z. Zhu, P. G. Evans, R. F. Haglund, and J. G. Valentine, "Dynamically reconfigurable metadevice employing nanostructured phase-change materials," Nano Lett. **17**(8), 4881–4885 (2017).
11. F. J. Morin, "Oxides which show a metal-to-insulator transition at the neel temperature," Phys. Rev. Lett. **3**(1), 34–36 (1959).
12. V. R. Morrison, R. P. Chatelain, K. L. Tiwari, A. Hendaoui, A. Bruhács, M. Chaker, and B. J. Siwick, "A photoinduced metal-like phase of monoclinic VO_2 revealed by ultrafast electron diffraction," Science **346**(6208), 445–448 (2014).
13. M. Imada, A. Fujimori, and Y. Tokura, "Metal-insulator transitions," Rev. Mod. Phys. **70**(4), 1039–1263 (1998).
14. O. L. Muskens, L. Bergamini, Y. Wang, J. M. Gaskell, N. Zabala, C. de Groot, D. W. Sheel, and J. Aizpurua, "Antenna-assisted picosecond control of nanoscale phase transition in vanadium dioxide," Laser Photonics Rev. **5**(10), e16173 (2016).
15. S. Wall, L. Foglia, D. Wegkamp, K. Appavoo, J. Nag, R. F. Haglund, J. Stähler, and M. Wolf, "Tracking the evolution of electronic and structural properties of VO_2 during the ultrafastphotoinduced insulator-metal transition," Phys. Rev. B **87**(11), 115126 (2013).
16. A. Cavalleri, C. Tóth, C. W. Siders, J. A. Squier, F. Ráksi, P. Forget, and J. C. Kieffer, "Femtosecond structural dynamics in VO_2 during an ultrafast solid-solid phase transition," Phys. Rev. Lett. **87**(23), 237401 (2001).
17. Y. Barkana and M. Belkin, "Laser eye injuries," Surv. Ophthalmol. **44**(6), 459–478 (2000).
18. A. Howes, Z. Zhu, D. Curie, J. R. Avila, V. D. Wheeler, R. F. Haglund, and J. G. Valentine, "Optical limiting based on huygens'metasurfaces," Nano Lett. **20**(6), 4638–4644 (2020).
19. C.-W. Qiu, T. Zhang, G. Hu, and Y. Kivshar, "Quo vadis, metasurfaces?" Nano Lett. **21**(13), 5461–5474 (2021).
20. M. L. Tseng, Y. Jahani, A. Leitis, and H. Altug, "Dielectric metasurfaces enabling advanced optical biosensors," ACS Photonics **8**(1), 47–60 (2021).
21. N. I. Zheludev and Y. S. Kivshar, "From metamaterials to metadevices," Nat. Mater. **11**(11), 917–924 (2012).

Optical Materials EXPRESS

22. P. Kepic, F. Ligmajer, M. Hrton, H. Ren, L. d. S. Menezes, S. A. Maier, and T. Šikola, "Optically tunable mie resonance VO_2 nanoantennas for metasurfaces in the visible," ACS Photonics **8**(4), 1048–1057 (2021).
23. A. Tripathi, J. John, S. Kruk, Z. Zhang, H. S. Nguyen, L. Berguiga, P. R. Romeo, R. Orobtchouk, S. Ramanathan, Y. Kivshar, and S. Cueff, "Tunable mie-resonant dielectric metasurfaces based on VO_2 phase-transition materials," ACS Photonics **8**(4), 1206–1213 (2021).
24. A. E. Serebryannikov, A. Lakhtakia, G. A. E. Vandenbosch, and E. Ozbay, "Transmissive terahertz metasurfaces with vanadium dioxide split-rings and grids for switchable asymmetric polarization manipulation," Sci. Rep. **12**(1), 3518 (2022).
25. T. Wang, J. He, J. Guo, X. Wang, S. Feng, F. Kuhl, M. Becker, A. Polity, P. J. Klar, and Y. Zhang, "Thermally switchable terahertz wavefront metasurface modulators based on the insulator-to-metal transition of vanadium dioxide," Opt. Express **27**(15), 20347–20357 (2019).
26. C. Wan, Z. Zhang, J. Salman, J. King, Y. Xiao, Z. Yu, A. Shahsafi, R. Wambold, S. Ramanathan, and M. A. Kats, "Ultrathin broadband reflective optical limiter," Laser Photonics Rev. **15**(6), 2100001 (2021).
27. E. Bermúdez-Ure na and U. Steiner, "Self-rolled multilayer metasurfaces," ACS Photonics **6**(9), 2198–2204 (2019).
28. C. Wan, E. H. Horak, J. King, J. Salman, Z. Zhang, Y. Zhou, P. Roney, B. Gundlach, S. Ramanathan, R. H. Goldsmith, and M. A. Kats, "Limiting optical diodes enabled by the phase transition of vanadium dioxide," ACS Photonics **5**(7), 2688–2692 (2018).
29. K. Appavoo and R. F. Haglund Jr., "Polarization selective phase-change nanomodulator," Sci. Rep. **4**(1), 6771 (2015).
30. C. Wan, Z. Zhang, D. Woolf, C. M. Hessel, J. Rensberg, J. M. Hensley, Y. Xiao, A. Shahsafi, J. Salman, S. Richter, Y. Sun, M. M. Qazilbash, R. Schmidt-Grund, C. Ronning, S. Ramanathan, and M. A. Kats, "On the optical properties of thin-film vanadium dioxide from the visible to the far infrared," Ann. Phys. **531**(10), 1900188 (2019).
31. Y. Wang, P. Landreman, D. Schoen, K. Okabe, A. Marshall, U. Celano, H. S. P. Wong, J. Park, and M. L. Brongersma, "Electrical tuning of phase-change antennas and metasurfaces," Nat. Nanotechnol. **16**(6), 667–672 (2021).
32. R. L. Olmon, B. Slovick, T. W. Johnson, D. Shelton, S.-H. Oh, G. D. Boreman, and M. B. Raschke, "Optical dielectric function of gold," Phys. Rev. B **86**(23), 235147 (2012).
33. I. H. Malitson, "Refraction and dispersion of synthetic sapphire," J. Opt. Soc. Am. **52**(12), 1377–1379 (1962).
34. D. Rocco, M. Gandolfi, A. Tognazzi, O. Pashina, G. Zograf, K. Frizyuk, C. Gigli, G. Leo, S. Makarov, M. Petrov, and C. De Angelis, "Opto-thermally controlled beam steering in nonlinear all-dielectric metastructures," Opt. Express **29**(23), 37128–37139 (2021).
35. A. Ronchi, P. Franceschini, P. Homm, M. Gandolfi, G. Ferrini, S. Pagliara, F. Banfi, M. Menghini, and C. Giannetti, "Light-assisted resistance collapse in a V_2O_3-based mott-insulator device," Phys. Rev. Appl. **15**(4), 044023 (2021).
36. A. Tognazzi, D. Rocco, M. Gandolfi, A. Locatelli, L. Carletti, and C. De Angelis, "High quality factor silicon membrane metasurface for intensity-based refractive index sensing," Opt. **2**(3), 193–199 (2021).
37. M. Gandolfi, S. Peli, M. Diego, S. Danesi, C. Giannetti, I. Alessandri, V. Zannier, V. Demontis, M. Rocci, F. Beltram, L. Sorba, S. Roddaro, F. Rossella, and F. Banfi, "Ultrafast photoacoustic nanometrology of InAs nanowires mechanical properties," J. Phys. Chem. C **126**(14), 6361–6372 (2022).
38. P. Kosky, R. Balmer, W. Keat, and G. Wise, "Chapter 14 - mechanical engineering," in *Exploring Engineering (Fifth Edition)*, P. Kosky, R. Balmer, W. Keat, and G. Wise, eds. (Academic Press, 2021), pp. 317–340, 5 edition ed.
39. J. Ordonez-Miranda, Y. Ezzahri, K. Joulain, J. Drevillon, and J. Alvarado-Gil, "Modeling of the electrical conductivity, thermal conductivity, and specific heat capacity of VO_2," Phys. Rev. B **98**(7), 075144 (2018).
40. A. Ronchi, A. Sterzi, M. Gandolfi, A. Belarouci, C. Giannetti, N. Del Fatti, F. Banfi, and G. Ferrini, "Discrimination of nano-objects via cluster analysis techniques applied to time-resolved thermo-acoustic microscopy," Ultrasonics **114**, 106403 (2021).
41. S. Burghartz and B. Schulz, "Thermophysical properties of sapphire, AlN and $MgAl_2O_4$ down to 70 K," J. Nucl. Mater. **212-215**, 1065–1068 (1994).
42. M. Gandolfi, F. Banfi, and C. Glorieux, "Optical wavelength dependence of photoacoustic signal of gold nanofluid," Photoacoustics **20**, 100199 (2020).
43. M. Celebrano, D. Rocco, and M. Gandolfi, *et al.*, "Optical tuning of dielectric nanoantennas for thermo-optically reconfigurable nonlinear metasurfaces," Opt. Lett. **46**(10), 2453–2456 (2021).
44. M. Qazilbash, M. Brehm, G. Andreev, A. Frenzel, P.-C. Ho, B.-G. Chae, B.-J. Kim, S. J. Yun, H.-T. Kim, A. Balatsky, O. G. Shpyrko, M. B. Maple, F. Kleimann, and D. N. Basov, "Infrared spectroscopy and nano-imaging of the insulator-to-metal transition in vanadium dioxide," Phys. Rev. B **79**(7), 075107 (2009).